

Effect of Paramagnetic Iron on Quantitation in Carbon-13 Cross Polarization Magic Angle Spinning Nuclear Magnetic Resonance Spectrometry of Heterogeneous Environmental Matrices

Philip E. Pfeffer,* Walter V. Gerasimowicz,* and Edwin G. Piotrowski

Eastern Regional Research Center, Agricultural Research Service, U.S. Department of Agriculture, Philadelphia, Pennsylvania 19118

¹³C solid state cross polarization magic angle spinning (CPMAS) spectra and proton relaxation parameters of model sludge components and derived mixtures were examined. Relative magnetization responses of lipid, carbohydrate, protein, and lignin components as well as their proton T_1 (spin-lattice relaxation times) and $T_{1\rho}$ (rotating frame spin-lattice relaxation times) values were evaluated in the presence of paramagnetic Fe^{3+} at levels found in whole sludge samples. Significant reductions in proton T_1 and $T_{1\rho}$ values were observed specifically in the hydrophilic components, suggesting that intimate contact of paramagnetic centers is felt through the more acidic exchangeable proton sites. Samples from each stage of the Beltsville sludge composting process were examined for total carbon content, composition, and the effect of paramagnetic metal by their ¹³C CPMAS spectra and proton relaxation times. Increases in residual lignified and aromatic components were followed by application of an interrupted decoupling sequence.

Application of anaerobically digested composted sludge to soils has been shown to be an effective method for producing plant-available N, P, and S (1), as well as a means for inducing the migration of neutralizing equivalents of calcium ions through the soil profile (2). Metal complexing groups found in the poorly defined fulvic and humic acid polymer networks of these materials (3, 4) can be a source of beneficial trace metals for the plant (e.g., Ca, Fe, Mg) (5). However, potentially hazardous heavy metals (e.g., Cd, Pb, Cr) (3, 6) may also be present. The delivery of any of these metals to the site of the plant host is dependent upon many factors including the state (inner or outer sphere complexes) (7-9), stability (7, 8), and solubility (9) of the complexes formed within the composted sludge matrix.

¹³C and ¹H solution NMR spectra of humic substances extracted from both soil (10) and sludge (4) provide qualitative information about the intact systems from which they are derived. However, the harsh alkaline extraction procedure required to obtain these materials leaves some doubt as to the interpretation of the data (11). Resolution and identification of aliphatic and aromatic carboxyl groups as well as phenols, aliphatic hydroxyl, and amino group functionalities (12, 13) in humic substances may be improved by ¹³C enrichment and permethylation.

Development of solid state ¹³C cross polarization magic angle spinning (CPMAS) NMR spectrometry (14, 15) has brought about the feasibility of examining intact matrices obviating the need for harsh chemical treatment. Numerous analytical applications of ¹³C CPMAS NMR spectrometry to the study of whole soils (16-19), humic (20, 21, 9) and fulvic

acids (22), humins (23), and sludge (24) have recently appeared.

We have addressed three questions concerning the use of ¹³C CPMAS NMR spectrometry as a tool for the quantitative evaluation of highly diverse matrices such as sludges. (1) What is the degree of resolution which may be achieved among the component types present in multicomponent model mixtures? (2) What is the range of relaxation values (proton T_1 's and $T_{1\rho}$'s) exhibited by such a heterogeneous mixture, and under optimum conditions, how does the known relative composition compare to the observed relative integrated intensities? (3) What are the effects of paramagnetic impurities, such as Fe^{3+} , on the observed spectral intensities and proton relaxation times of various resonances representing each component of the system?

EXPERIMENTAL SECTION

NMR Spectrometry. NMR spectra were obtained with a JEOL FX-60QS NMR spectrometer operating at a ¹³C frequency of 15 MHz. The ¹H decoupling rf irradiation field strength was 11 G. A spectral width of 8000 Hz and a sampling of 2K data points zero filled to 8K was used throughout. Chemical shifts were assigned relative to tetramethylsilane in a sealed capillary using hexamethylbenzene (HMB) as a secondary reference with a shift position of 17.36 ppm for the CH₃ peak. Each spectrum of sludge required from 10 000 to 40 000 scans depending on the carbon content. (Sludge mixtures should be handled with care in a well ventilated hood with protective clothing.) Samples were spun at approximately 2.1 kHz. No spinning sidebands were noted. Measurement of all areas was done in triplicate with a planimeter.

Relaxation Studies. Peak intensity measurements were used for the calculation of relaxation times (T_{1H} 's and $T_{1\rho H}$'s). Each frequency domain spectrum was obtained with 40 Hz of computer line broadening. Values of T_{1H} were obtained by observation of the ¹³C magnetization via cross polarization in the 180°-τ-90° pulse sequence (25). Values of $T_{1\rho H}$ were measured by the loss of ¹³C magnetization as a function of increasing contact times (26). Both T_{1H} and $T_{1\rho H}$ were calculated by a two-parameter exponential fit of the relaxation data. A double exponential fit was used for the analysis of the proton $T_{1\rho}$ and T_{CH} (carbon-proton cross polarization time) values for keratin and wood pulp. The uncertainty in the calculated values was generally found to be ±10%. Correct representative intensities of our standard CPMAS spectra were obtained by measuring the observed intensity responses of each component as a function of both contact time and recycling time. In the spectra of the model multicomponent system, maximum carbon magnetization was realized at a contact time of 0.5 ms and a recycling time of 20 s. No measurable difference in relative carbon intensities was noted in the sludge mixtures using recycling times of 1.5 s or 20 s. Interrupted ¹³C-¹H decoupling experiments, designed to accentuate the nonprotonated ¹³C resonances, were also performed (27). A 40-μs delay without proton decoupling was inserted into the pulse sequence prior to data acquisition.

Model Sludge Mixture. The model mixtures were prepared

by adding 1.350 g (67.5%) of wood pulp, 0.300 g (15%) of keratin, 0.250 g (12.5%) of stearic acid-palmitic acid 1/1, and 0.100 g (5%) of lignin to a 300-mL lyophilizing flask containing 100 mL of deionized water. The mixture was gently shaken at room temperature on a mechanical shaker at 60 cycles/min for 2 h. The iron-spiked samples were prepared as above with the addition of 0.200 g of $\text{FeCl}_3 \cdot 6\text{H}_2\text{O}$ to the flask prior to shaking.

Wood Pulp/ Fe^{3+} Mixtures. Wood pulp was ground in a Wiley mill. The material was passed consecutively through a 3 mm screen, a 20 mesh screen, and a 40 mesh screen. This freshly ground and sieved wood pulp was lyophilized overnight to constant weight. One-gram samples of the lyophilized wood pulp were added to each of five, 250-mL glass-stoppered flasks. $\text{FeCl}_3 \cdot 6\text{H}_2\text{O}$ was added to each sample as follows: 0.00 mg; 0.15 mg; 1.50 mg, 15.00 mg; and 150.00 mg. Each of these samples was made up to 100 mL with deionized water. The samples were shaken at 100 rpm in a 25 °C water bath for 2 h. These mixtures were dried to constant weight on a lyophilizer. The total concentration of iron in these samples was determined by atomic absorption.

Sludge and Compost Samples. Samples were obtained at each stage of the sludge treatment and composting process of the Philadelphia Water Department Southwest Sludge Processing Facility. Their treatment system employs a procedure developed by the U.S. Department of Agriculture known as the Beltsville Method (28). All samples were lyophilized to constant weight. Freeze-dried samples from stages 4 through 7 inclusive (see below) were then ground with a micromill and passed through a 35 mesh sieve in order to provide as homogeneous a mixture as possible. These materials were stored under refrigerated conditions until required for experimental use.

Description of Processing Stages Sampled. *Stage 1: Wastewater.* Untreated sewage was sampled which had passed through bar screens to remove large debris (>1 in.). Heavy inorganics and organics with specific gravities >2 are removed by sedimentation in these grid tanks and the resultant product is primary sludge.

Stage 2: Anaerobic Digestion. The primary sludge is pumped to anaerobic digestion tanks where microbial action results in conversion of organic material to volatile acids, methane, and carbon dioxide.

Stage 3: Dewatering. After digestion, the sludge is dewatered by mixing and centrifugation with a bulking agent (Percol 728, Allied Colloids, Inc., Fairfield, NJ). The flocculating polymer is added at ca. 6 to 7 lb/ton of dewatered mix produced during this step. The anaerobic digest enters the dewatering process at 4% to 5% solids and is discharged at 20% to 25% solids.

Stage 4: Mixing. The dewatered sludge cake was mixed with wood chips. Compost is obtained through mixing approximately two parts of wood chips to one part of dewatered substance on a volume basis. Vigorous mixing action of the wood chips and sludge cake is accomplished mechanically by front-end loaders.

Stage 5: 21-Day Compost. The combined sludge and wood chip mix was placed in a compost pile built on a 1 in. bed of wood chips. A loop of 4 in. plastic perforated pipe has been placed on the bed of wood chips. Air is drawn through the pile with blowers in order to dry the material and increase the temperatures in the compost piles. The blowers were run on a 50% on, 50% off cycle. Temperatures are monitored throughout these piles to maintain minimum readings of 148 °F to destroy pathogens which may be present.

Stage 6: Cured Compost. After 21 days the compost piles are dismantled and trucked to storage areas for 3 months of further drying.

Stage 7: Screened or Finished Compost. Wood chips were removed by running cured compost through compost screens. The wood chips are recovered and recycled while the screened compost becomes the final product of the entire treatment process.

Humic and Fulvic Acids. Standard procedures were employed in isolating humic and fulvic acid fractions from samples of the anaerobic digest (stage 2), and final compost product (stage 7) of the Philadelphia Water Department Southwest Sludge Processing Facility (29). All samples were filtered through DIAFLO UMO5 ultrafiltration membranes, washed, and dried prior to examination.

Atomic Absorption Metal Determinations. All metal concentrations were determined by standard methods on a

Perkin-Elmer 5000 atomic absorption spectrophotometer.

RESULTS AND DISCUSSION

CPMAS Methodology. In order to obtain natural abundance ^{13}C spectra of solids of high resolution quality approaching that of solution spectra, the following techniques are utilized (14, 15, 26): (1) high power dipolar decoupling of the proton spins to eliminate the ^{13}C - ^1H dipolar interactions associated with ^{13}C line broadening, (2) matching of the abundant ^1H spin and dilute ^{13}C spin rotating frame Larmor frequencies to induce cross polarization-energy transfer to overcome low sensitivity associated with long ^{13}C spin-lattice relaxation times and low ^{13}C natural abundance, (3) rapid sample spinning about the "magic angle" of 54.7° to eliminate heteronuclear dipolar interactions and large chemical shift anisotropy due to rigid molecular orientation in the lattice.

Spectral dissimilarities among various sludge samples may reflect true differences in the ratio of various components and/or differences in the proportional proton cross polarization response for the different carbon types present (24). Since these systems contain large quantities of paramagnetic metals, the question of heterogeneous metal distribution throughout this matrix gives further cause for concern in that such species may affect various relaxation mechanisms, and consequently the observed relative quantitation via ^{13}C resonance intensity (24, 25, 30, 31).

Of the three experimental techniques for obtaining CPMAS spectra mentioned above, the second is most critical for controlling the relative magnetization or intensity response exhibited by the ^{13}C resonances. Complete cross polarization (energy exchange) relies on slow proton rotating frame relaxation processes to facilitate the ^{13}C responses. Because the abundant protons in organic solids are close together, rapid spin diffusion may occur among them. This process allows all protons within an individual component to have the same relaxation behavior. If spin diffusion is not uniform throughout the sample due to heterogeneity, the proton relaxation processes can differ for each component. As a result of this nonuniform distribution of the proton population in our multicomponent systems, $T_{1\rho\text{H}}$ differences become readily apparent under high-resolution conditions. The success of the cross polarization process depends upon the relative rate of carbon-proton cross polarization, T_{CH} (the time required for energy exchange between the carbon to proton populations), as well as the rate of the competing process which reflects the loss of proton polarization, proton $T_{1\rho}$ (the spin-lattice relaxation time in the rotating frame). The relative rates of these two processes determine the extent of complete ^{13}C polarization and subsequent attainment of proportional ^{13}C intensity response. To achieve these ends the T_{CH} should be considerably shorter than the time constant, $T_{1\rho}$, associated with the loss of proton polarization. The optimal experimental contact time (cross polarization time) should be appreciably smaller than proton $T_{1\rho}$ so that the spin-locked proton magnetization does not relax during the energy transfer period. In all of the model systems and intact matrices presented in this paper, T_{CH} values will be extremely rapid owing to large populations of directly bonded and nearest neighbor protons. Consequently, the acquisition of quantitative results will depend primarily on the relative ^{13}C responses dictated by the range of proton T_1 and proton $T_{1\rho}$ values of the various components. Careful selection of recycling and contact times, respectively, is therefore required.

Sludge Model System. To establish the relative response of various components in a heterogeneous matrix such as sludge, we initially examined a model multicomponent mixture (previously described) (24). We do not wish to imply that the components which make up the model mixture are the only components present in sludges. These model constituents

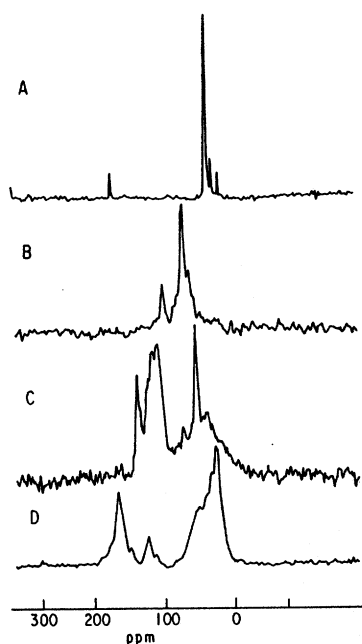


Figure 1. CPMAS ^{13}C NMR spectra of reference compounds: (a) stearic acid, (b) wood pulp, (c) lignin, and (d) keratin. Each spectrum was obtained from 3000 acquisitions with a pulse delay of 1.5 s and a contact time of 0.5 ms and 10–15 Hz line broadening.

Table I. Relaxation Values^a of Model Components

component	Fe^{3+} ^b		without Fe^{3+}	
	$T_{1\text{H}}$	$T_{1\rho\text{H}}$	$T_{1\text{H}}$	$T_{1\rho\text{H}}$
wood pulp	3.0	2.2	78.8	7.0
lipids	2.5×10^3	18.6	5.0×10^3	21.0
protein	9.1	3.8	83.0	4.7
lignin	73.0	7.3	164.0	7.0
microcrystalline cellulose	2.0	7.3	505.0	

^a Milliseconds \pm 10%. ^b 1.9%.

were selected to represent the predominant carbon types evident in the spectra of the sludges presented in this work. Prior to making these measurements we evaluated the relaxation values (proton T_1 and $T_{1\rho}$) of the individual compounds used to prepare the model system (Figure 1 shows the ^{13}C CPMAS spectra of each component used). The range of relaxation parameters was also measured in the presence of paramagnetic Fe^{3+} (in concentrations approximating sludge), to note its effect on each type of component. Table I lists the proton T_1 and $T_{1\rho}$ values for the individual components in both the presence and absence of Fe^{3+} . All of these samples were prepared in a somewhat amorphous state by lyophilization from water. The final state of the lipid fatty acid component in the model mixture appears to be somewhat more ordered than that of the other model compounds as evidenced by its extremely long T_1 and $T_{1\rho}$ values. The T_1 and $T_{1\rho}$ values associated with this hydrophobic component exhibit little change when the paramagnetic-amended system is compared to the analogous non-iron-containing mixture. Similarly, the hydrophobic nature of lignin does not foster intimate spatial communication with the Fe^{3+} since its T_1 has only diminished by half while its $T_{1\rho}$ has essentially remained the same. The more hydrophilic carbohydrate and protein constituents of the model do, however, show signs of significant interaction with the paramagnetic centers. Iron-induced shortening of T_1 is evident in both the protein and carbohydrate. Researchers have exploited this concept through the addition of small quantities of paramagnetic species to pure peptides thereby reducing their proton T_1 's and recycling times

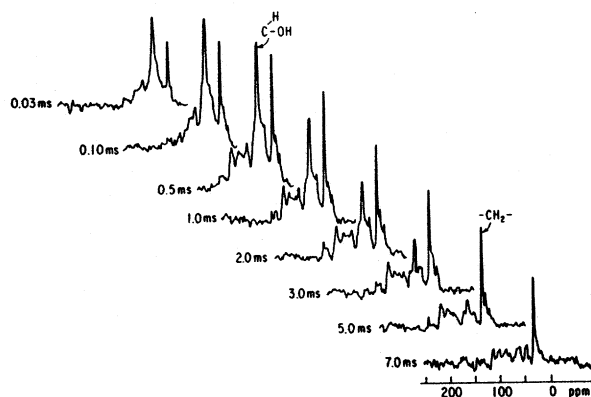


Figure 2. Contact time study of model sludge mixture containing 1.9% Fe^{3+} . Each spectrum was obtained after 5000 scans, a pulse delay of 1.5 s, contact times of 0.03 ms to 7.0 ms, and 15-Hz line broadening.

while simultaneously enhancing the efficiency of the CPMAS experiment (30, 31). Such preferential shortening of T_1 can have a pronounced effect on ^{13}C sensitivity when one uses a recycling time of 4–5 T_1 's. In our example, the large spread of proton T_1 values necessitates the use of pulse delay values of 20 s and 10 s, respectively, in the absence and presence of 1.9% Fe^{3+} to ensure reestablishment of nearly total proton equilibrium magnetization.

The rate of proton relaxation, $T_{1\rho}$, presents a different problem when trying to establish equal carbon population responses. A contact time must be selected which will be fast enough to facilitate carbon-proton energy transfer for the components with rapidly relaxing protons (short $T_{1\rho}$'s) as well as those with long $T_{1\rho}$ values (25, 32). This question has been addressed in a paper concerning the analytical reliability of the solid-state ^{13}C spectra of coals (25). Yoshida et al. examined the effect of pulse repetition rates and contact times on the ^{13}C solid-state spectra of a coal sample and a hexane-soluble fraction (33). Optimal contact times and pulse delays were required to obtain reliable estimates of carbon aromaticity in their samples (34). Unlike the heterogeneous models and sludges examined in the present study, the coal samples contained carbon compounds of limited diversity, e.g., aliphatic and aromatic hydrocarbons, with a relatively narrow range of proton $T_{1\rho}$ values. As seen in Table I, the dynamic range of $T_{1\rho}$ values in the present study is exceedingly large even for the metal-free components (\sim 7.0 ms to 21.0 ms).

In order to maximize the absolute ^{13}C responses of the model mixture, we performed a study of the contact time vs. intensity of our model mixture in the presence and absence of Fe^{3+} as found in sludge mixtures. In these systems, with and without Fe^{3+} , we observed the rapid growth of the carbohydrate resonances at \sim 70 ppm and 102 ppm as well as the aliphatic resonances at \sim 30 ppm in the range of contact times 0.03 ms to 0.5 ms. From 0.5 ms to 7.0 ms there is a rapid loss of signal from the carbohydrate peaks while the aliphatic peak, having long $T_{1\rho}$ values (21.0 ms no Fe^{3+} , 18.6 ms Fe^{3+}), clearly persists. Cross-relaxation effects on the protein and lignin resonances are more difficult to assess because of their overlap with each other and with the aliphatic region. For both the metal- and nonmetal-containing samples, the maximum response for both components (lipid and carbohydrate) is found at a contact time of ca. 0.5 ms. Figure 2 illustrates the generation of carbon magnetization for the Fe^{3+} -containing model system as a function of variable contact time. At the shorter contact times ($<$ 0.5 ms) necessary to overcome the rapid proton relaxation process, the relationship of $T_{\text{C-H}} \ll$ contact time becomes invalid and loss of absolute ^{13}C intensity is apparent. This phenomenon is clearly illustrated when we examine the spectra of the model mixture under optimum

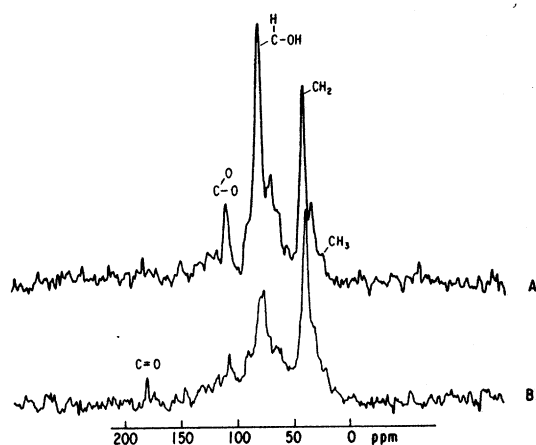


Figure 3. Comparison of ^{13}C CPMAS NMR spectra of model sludge mixtures (a) with no Fe^{3+} and (b) containing 1.9% Fe^{3+} . Each spectrum was obtained under the optimized conditions, 14 000 scans, 16-s pulse delays, a 0.5-ms contact time, and 20-Hz line broadening.

conditions with and without metal as seen in Figure 3. In spectrum 3A we see that the ratio of the carbohydrate resonances at ~ 102 ppm and ~ 70 ppm (corrected for lignin content) to the aliphatic region at ~ 30 ppm is $(2.2/1.0) \pm 10\%$ (theory 2.1/1). Spectrum 3B in the presence of 1.9% Fe^{3+} with the aliphatic region normalized to the aliphatic region of 3A shows a ratio of carbohydrate/lipid of only $(1.1/1.0) \pm 10\%$. From these data it is obvious that even under these most optimum conditions of short contact times of 0.5 ms and long recycling times of 20 s, 48% of the carbohydrate signal has been lost. At these high Fe^{3+} concentrations (1.9%) we observe preferential loss of proton polarization associated with the carbohydrate species. The Fe^{3+} concentration dependence of the phenomenon can be seen in Table I.

The lost ^{13}C intensity is due to the loss of magnetization for those carbons that have severely diminished $T_{1\rho}$ values relative to their corresponding cross-relaxation times (T_{CH}). While ^1H spin polarization is being transferred to all of the components in the model, the short proton $T_{1\rho}$ associated with the carbohydrate component upon paramagnetic doping causes a loss in its signal intensity much more rapidly than any decay seen in the other constituents with their longer proton $T_{1\rho}$'s. The regime of $T_{\text{CH}} \ll \text{contact time} \ll T_{1\rho\text{H}}$ is difficult to meet in our model system for the carbohydrate component in the presence of large quantities of paramagnetic iron. This effect is reflected in the wide dynamic range of proton $T_{1\rho}$ values seen in Table I. If one cannot account for all carbon in a sample in an absolute sense, the fraction of carbon resonances must at least be representative of all carbon in the sample.

Cross Polarization and Relaxation Studies of Wood Pulp and Keratin Samples. The specific generation of ^{13}C magnetization in wood pulp samples, with and without iron addition, was also examined. The loss of carbohydrate signal at certain contact times, as well as the specific change in the ratio of the carbohydrate resonances to the other component resonances in the spectra of the model mixture upon paramagnetic doping, prompted further investigation of the wood pulp alone. The dependence of the ^{13}C CPMAS amplitude for the carbohydrate resonance (ca. 73 ppm) as a function of the Hartman-Hahn contact time is depicted in Figure 4A. Similar spectral and calculated data are shown for keratin in Figure 4B. The growth of the ^{13}C signal amplitude is dependent upon the carbon-proton cross polarization rate, T_{CH} . The decline in amplitude, which manifests itself at longer contact times, is due to ^1H spin-lattice relaxation in the rotating frame, $T_{1\rho\text{H}}$. Literature methods were employed in treating the data by means of least-squares refinement and

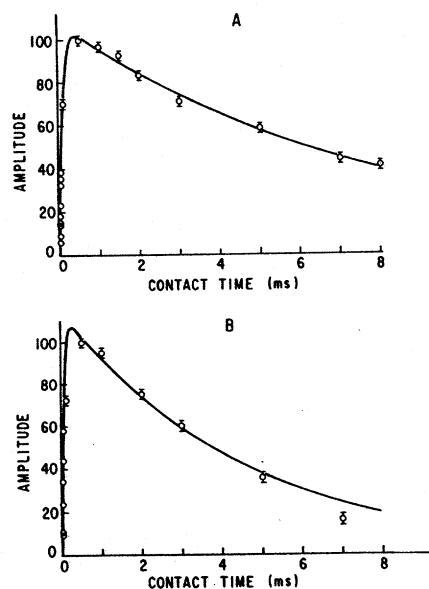


Figure 4. Plot of ^{13}C CPMAS amplitude (relative intensities) vs. contact time: (A) wood pulp (73 ppm resonance); (B) keratin (30 ppm resonance).

Table II. Relaxation Values^a of Wood Pulp^b and Keratin^c

$\text{Fe}^{3+ d}$	$T_{1\text{H}}$	$T_{1\rho\text{H}}$	$T_{\text{C-H}}^e$
Wood Pulp			
25400	2.9	2.7	
2860	13.1	5.8	
419	53.2	6.5	
184	79.0	6.9	
153	78.8	8.2	0.087
Keratin			
	83.0	4.5	0.056

^a Milliseconds $\pm 10\%$. ^b Carbohydrate region of ^{13}C spectra at ca. 75 ppm. ^c Region of ^{13}C spectra at ca. 35 ppm. ^d Parts per million. ^e $\pm 25\%$.

curve fitting (26). The results are seen in Table II. Analogous results for keratin are also specified in Table II. No experiments on keratin/ Fe^{3+} doped samples were carried out as part of this study.

In the case of the wood pulp where no ferric chloride has been added, a trace of iron is found in the sample (153 ppm; Table II). This minute percentage of iron does not affect the first-order exponential decay or $T_{1\rho\text{H}}$ fit of the experimental data whose value is 8.2 ms. However, in the wood pulp samples where paramagnetic iron has been added, initial non-first-order decay may have been detected. This initial non-linear decay may be a function of differential spin diffusion or phase separation where paramagnetic effects are being detected more rapidly by protons, and thus carbon atoms, in the immediate vicinity of the metal ion. Thus, incomplete averaging of the proton $T_{1\rho}$'s may have been observed as a consequence of incomplete spin diffusion. Therefore, experimental intensities at slightly longer contact times, resulting in linear slopes, were used in our least-squares refinements. The relaxation values for these iron-spiked materials listed in Table II are indicative of apparent or average cross-relaxation times.

The apparent proton $T_{1\rho}$ values for the wood pulp samples in Table II decrease as the concentration of Fe^{3+} increases. The paramagnetic influence on this parameter is very dramatic at the higher levels of iron approximating those seen in sludges. We note in Figure 4 that an optimal contact time of ap-

Table III. Selective Elemental Analysis of Samples from the Various Stages of Sewage Treatment

stage	% C	% H	% N	% S
1. raw sewage	36.04	5.68	3.60	0.97
2. anaerobic digest	28.04	4.47	3.16	
3. centrifuged digest	27.24	4.30	3.18	
4. mix (sludge + wood chips)	40.30	5.36	1.67	
5. 21-day compost	40.71	5.69	1.22	
6. 3-month compost	33.79	4.73	1.37	
7. screened compost	25.83	3.75	1.85	0.60

proximately 0.4–0.5 ms is required in order to generate maximal signal responses from all visible, protonated carbon resonances. For the pure wood pulp, $T_{1\rho}$ is approximately 16.4 times longer than the optimal contact time determined graphically. For the sample with 25 400 ppm of Fe^{3+} , the $T_{1\rho}$ is 5.4 times longer than a 0.5-ms contact time. The overall observed shortening of the measurable $T_{1\rho}$ suggests that a significant amount of the ^{13}C magnetization is being lost before full transfer of spin polarization can be effected. The iron which was added to these wood pulp samples was initially in a paramagnetic form. The rapid relaxation rates observed at the high iron concentrations imply that most of the added iron has remained in a paramagnetic state, i.e., the electronic charge is not delocalized through ionic association or formation of complexes with the wood pulp. Large concentrations of paramagnetic centers will shorten the macroscopic $T_{1\rho}$'s observed relative to cases with lower amounts of paramagnetics, and probably broaden and shift a fraction of the ^{13}C resonances outside of the instrumental detection range. This result further confirms the reason for the relative loss of carbohydrate intensity in the model system above.

The Sludge Process. In this study we have profiled the progress of the Beltsville sludge-composting process (28) with ^{13}C CPMAS NMR methodology, keeping in mind the limitations put on the technique with respect to the extreme heterogeneity of the mixtures being examined. Table III gives a profile of the C, H, N, and S content of the material as it evolves through the process. From stage 1 to 3 a continual breakdown of organic matter is occurring as evidenced by a 24% drop in the carbon content. During these same stages, nitrogen decreased slightly (ca. 12%) suggesting the presence of inorganic or nonproteinaceous nitrogen-containing compounds that are resistant to degradation. Upon addition of wood chips in stage 4, the system becomes high in organic carbon and lower in nitrogen. Three months of composting causes significant organic breakdown (17% loss of carbon from stage 4 to stage 6) as well as an increase in oxidized or humified material. This trend is indicated by a C/H weight ratio of 7.1 for stage 7 vs. 6.3 for stages 1 and 2.

Table IV lists the observed changes in the metal content of the sludge compost at each stage of the process. We note that Fe, Ca, and Al are the three most abundant metals found in the raw material and final product. Fe, Ca, and Al, unlike the Na and K, do not become appreciably solubilized after flocculation in step 3. We assume that the latter groups are bound tightly. This group (Fe, Ca, and Al) of metals appears

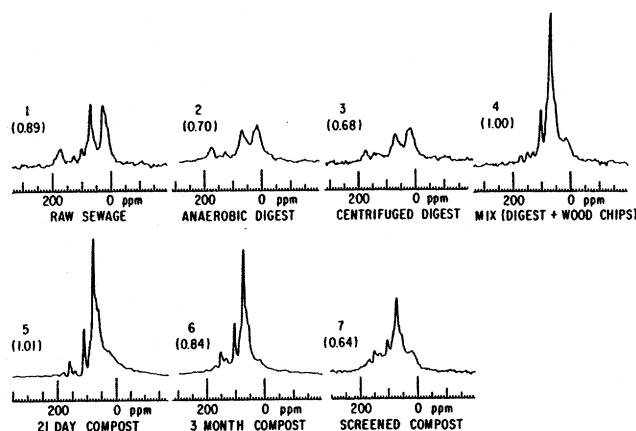


Figure 5. ^{13}C CPMAS spectra of the seven-stage sludge-composting process. Each spectrum was the result of 40 000 scans, a pulse delay of 1.5 s, a contact time of 0.5 ms, and 40 Hz line broadening. The numbers in parentheses are the integrated carbon intensity of each spectrum normalized to the spectrum of stage 4.

to be bound to the organic matrix as observed with fulvic acid or polyelectrolyte components from soils (8).

After centrifugation and dewatering of the anaerobic digest (stage 3) the treatment process is not designed to further remove inorganic salts or metals from the sludge. We note in Table III that the total percentage of C in stage 3 is not very different from that seen in stage 7. Although the total amount of C has not changed drastically, the relative concentrations of carbon functionalities have changed quite markedly. The concentration of Fe drops by ca. 37% when comparing stage 3 to stage 7. A similar reduction of ca. 29% is noted in the Al concentration when stage 3 and stage 7 of the process are examined. These results imply that the cellulosic wood chips probably exhibit a preferential interaction for Fe and Al in that binding or association of these metals to the cellulose, which is removed at stage 6, produces the observed reductions. In contrast, Ca and Mg exhibit increases in their detectable concentrations of ca. 21% and 163%, respectively, when the same comparison is made. These increases indicate that Ca and Mg are preferentially complexed by the compost matrix before removal of excess wood at stage 6. The other metal distributions listed in Table IV may be similarly examined. Thus, other heavy metals show differential degrees of binding to the carbohydrate or hydrophilic components present in compost. For example, the concentrations of Mn and Cu remain relatively stable throughout the process while the toxic metals Cr and Cd have both diminished by approximately 60%.

NMR Evaluation of Intact Sludge Compost. Sludge fractions were evaluated by ^{13}C CPMAS NMR using the optimized parameters established for the heterogeneous model system. Although a contact time of 0.5 ms was used in this study, a recycling time of only 1.5 s was necessary since the length of proton T_1 values was considerably shorter. Figure 5 illustrates the progress of the sludge process as a function of ^{13}C resonance response. The values in parentheses represent

Table IV. Distribution of Selected Metals in Samples from the Various Stages of Sewage Treatment^a

stage	Fe	Mg	Ca	Zn	Na	K	Cu	Mn	Al	Cr	Cd
1. raw sewage	13 700	2500	19 700	1390	2520	2510	903	359	11 500	935	20.4
2. anaerobic digest	27 100	3040	25 800	1970	1940	2220	1120	506	13 300	990	25.8
3. centrifuged digest	28 400	2590	24 200	2000	518	819	1080	499	13 800	1000	24.5
4. mix (sludge + wood chips)	8 980	1520	12 300	665	317	1670	486	188	4 680	308	7.9
5. 21-day compost	6 940	1030	10 700	590	148	1460	443	157	3 970	255	6.9
6. 3-month compost	11 900	2710	18 500	865	306	1600	554	287	5 990	337	7.6
7. screened compost	17 900	6810	29 400	1432	295	2060	677	477	9 830	519	12.1

^a Ppm metals in samples on a dry weight basis.

Table V. Normalized ^{13}C Resonance Areas^a for Stages 1-7

resonance position (ppm)	stage 1	stage 2	stage 3	stage 4	stage 5	stage 6	stage 7
32 (CH_2, CH_3 , protein)	1.00	1.00	1.00	1.00	1.00	1.00	1.00
74 (C-O, carbohydrate)	0.84	0.64	1.09	4.75	1.97	3.46	1.48
131 (aromatic)	0.16	0.19	0.39	0.59	0.18	0.67	0.47
181 (C=O)	0.23	0.16	0.28	0.12	0.06	0.11	0.35

^a Determined by planimetry.

Table VI. Proton T_1 and ($T_{1\rho}$) Values^a for Aliphatic Carbons of Stages 1-3

resonance position	stage 1	stage 2	stage 3
32 ppm ^b (CH_2 , CH_3 , protein)	31.4 ± 11 (12.3 ± 1.6)	18.4 ± 2.8 (5.8 ± 0.5)	18.2 ± 2.5 (7.3 ± 0.7)

^a Milliseconds. ^b Average value obtained from peak height of the broad resonance centered at 32 ppm.

the relative area of carbon, normalized to stage 4 under each spectrum. In terms of the progressive degradation process, the values of the corresponding ^{13}C intensities compare favorably with the known carbon contents given in Table III. The fact that the relative integrated carbon resonance areas agree with the elemental analyses for the various treatment stages depicted further corroborates the choice of contact time and demonstrates that quantitative spectral results may be obtained even on highly diverse, heavy-metal-containing systems. We note that the finished product is lower in overall carbon content even though a large amount of carbon has been added as wood chips at stage 4.

Table V gives a profile of each carbon type represented in the spectrum at each stage of the process assuming equal response factors for all components. The area of each broad resonance band was measured by planimetry (after dropping lines between peaks to the base line) and normalized to the resonance area centered at 32 ppm. The resonance areas centered at 32 ppm correspond to aliphatic CH_2 and CH_3 groups and 73% of the proteinaceous carbon intensity (estimated from the keratin spectrum), 74 ppm corresponds to C-OH and carbohydrate ring carbons, 131 ppm to aromatic carbons from lignin and aromatic amino acids, and 181 ppm to ester, amide, and fatty acid carbonyls, respectively. During the initial stages of anaerobic degradation (stages 1-3), we observe an increase in the amount of oxidized and aromatic resonance (74 ppm and 131 ppm). Upon addition of wood chips the peak at 74 ppm dominates the spectrum. We also see a significant increase in the aromatic region. By the final stage, the composition of the mixture has changed significantly from the initial feed. The amount of oxidized carbon (C-O) has increased by 78%, aromatic carbon has tripled, and the carbonyl components have shown a 50% increase relative to the concentration of carbons representing the aliphatic region.

Figure 6 shows a more detailed picture of the initial and final product in terms of the relative composition of its component materials. The initial feedstock, Figure 6A, shows a large amount of aliphatic material in the range from 14 to 32 ppm as well as an almost equal amount of oxygen-bonded carbons (almost exclusively carbohydrate ring carbons at 73 ppm and anomeric carbons at 106 ppm). Carbonyl group absorptions from lipid and proteins are observed in a broad centered at 179 ppm. A small amount of aromatic carbon is seen at 130 ppm. Little change in these ratios takes place until the addition of wood chips at stage 4, whereupon the carbohydrate resonances at 73 ppm and 106 ppm dominate the spectrum. Even after lengthy microbial action and separation of the extraneous wood chips, the carbohydrate components still dominate the product, Figure 6B. Also we see an increase in the lignin as evidenced by the appearance of the OCH_3 resonance of ~57 ppm and the nonprotonated aromatic carbon resonances at 153 ppm (see Figure 1 for comparison). To ensure that the carbon resonance responses are giving an

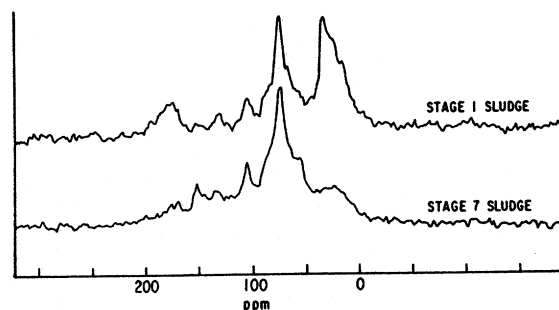


Figure 6. Detailed ^{13}C CPMAS spectra of stages 1 and 7 of the sludge-composting process taken under the conditions given in Figure 6.

Table VII. Relaxation Values^a of Carbohydrate^b in Beltsville Treatment Stages

stage	Fe ^c	T_{1H}	$T_{1\rho H}$
1	13 700	92.6	9.9
2	27 100	21.8	6.6
3	28 400	20.2	5.8
4	8 980	80.0	5.0
5	6 940	81.7	7.5
6	11 900	35.6	9.2
7	17 900	19.5	5.7
humic 2	662	53.0	3.8
		(60.2) ^d	(5.9) ^d
humic 7	5 858	3.9	2.1
		(3.9) ^d	(2.4) ^d
fulvic 2	5 340		
fulvic 7	10 178		

^a Milliseconds ± 10%. ^b Carbohydrate region centered at ca. 75 ppm. ^c Parts per million. ^d Aliphatic region centered at ca. 32 ppm.

accurate picture of the composition of these materials, we measured the range of proton relaxation times as described earlier for the model systems. Because of the large excess of carbohydrate (wood chips) introduced into the processing at stage 4, it was impossible to obtain accurate proton T_1 and $T_{1\rho}$ data for the noncarbohydrate aliphatic components beyond stage 3. The values listed in Table VI reflect a relative increase in Fe^{3+} content as a function of carbon loss due to anaerobic degradation. The relatively small changes in these values give a good indication that the high level of iron has little effect on the magnetization responses of this proton population as suggested in the model system. Relatively long $T_{1\rho}$ values assure us that the protons will be fully polarized during the cross polarization process. Table VII gives a range of both proton T_1 and $T_{1\rho}$ values for the carbohydrate component resonances throughout the entire process. This component was selected as a marker for the changes in relaxation behavior because of its demonstrated sensitivity to paramagnetic species

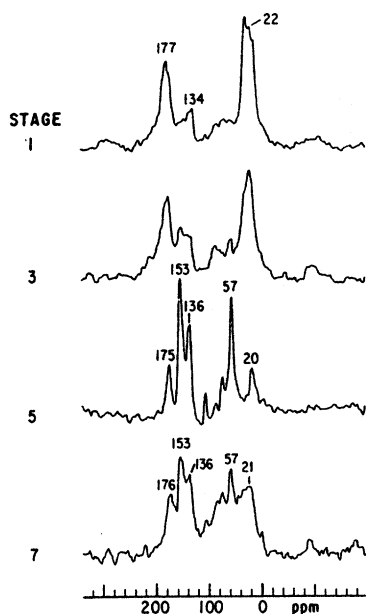


Figure 7. ^{13}C CPMAS spectra of stages 1, 3, 5, and 7 of the sludge-composting process taken under the selective broadening conditions of a 40- μs delay with no proton decoupling inserted into the pulse sequence prior to acquisition of the data.

in the model system. A comparison of both proton T_1 and $T_{1\rho}$ values with the Fe concentration profile shows a shortening of both $T_{1\text{H}}$ and $T_{1\rho}$ with increased Fe concentration for the first three stages. Upon addition of the excess carbohydrate in stage 4, the proton T_1 rose sharply, while $T_{1\rho}$ remained relatively constant. The downward trend in the proton T_1 from stages 5 through 7 parallels the consistent loss of carbon and the simultaneous increase in the relative concentration of iron. With the exception of stage 6, all of the $T_{1\rho}$ values show a decreasing trend with increasing iron concentration before and after the addition of wood pulp. The overall magnitude of the observed values of both relaxation times does not seem to reflect the level of paramagnetism exhibited by similar iron concentrations in the model wood pulp (compare with Table II). This disparity is most probably a consequence of Fe speciation within the matrix. Fe can exist in a diamagnetic state internally chelated in both inner or outer sphere complexes (7) in addition to its paramagnetic state. On the basis of our studies of wood pulp relaxation times as a function of paramagnetic iron concentration (Table II), we can estimate that there is virtually no paramagnetic influence on the carbohydrate resonance in stages 1 and 6. Stages 3 and 4 may contain as much as 10% and 32%, respectively, of the 28 400 and 8980 ppm of iron in a paramagnetic state (neglecting the small contributions of Cu and Cr). Insofar as quantitation is concerned, all of the $T_{1\rho}$ values for the sludge fractions meet the requirements of being much greater than the $T_{\text{C-H}}$ values previously determined for polymeric carbohydrates. Consequently, no significant amount of carbon magnetization is being lost for any of the spectra throughout the process.

Examination of Composting via Interrupted ^1H - ^{13}C Decoupling. To evaluate the distribution of the component parts of the intact sludge fractions in greater detail, we examined the dipolar ^{13}C broadened spectra in selected stages. This alteration has the effect of selectively broadening all carbon resonances that correspond to carbons having directly bonded protons (27). This experiment allows us to discriminate against the protonated carbons and selectively look at the nonprotonated ^{13}C population. Some methyl group resonances also remain in the spectrum because of the reduced C-H dipolar broadening due to the methyl group's rotational

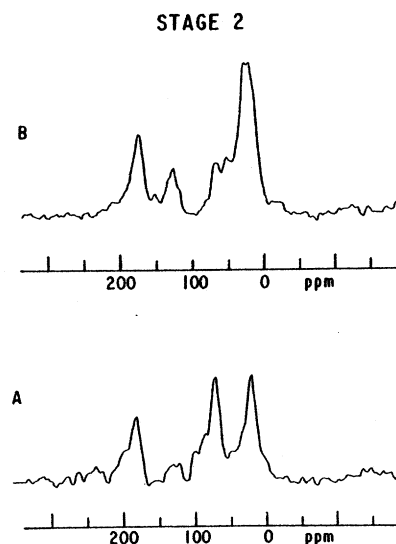


Figure 8. ^{13}C CPMAS spectra of (a) fulvic and (b) humic acid fractions from stage 2 of the sludge-composting process: (a) was taken with 50 000 scans, pulse delay of 1.5 s, a contact time of 0.5 ms, and line broadening of 40 Hz; (b) was obtained with 5000 scans, pulse delay 1.5 s, a contact time of 0.5 ms, and line broadening of 40 Hz.

motion. Figure 7 shows that for the anaerobically treated digest (stage 3), there are greater numbers of nonprotonated or oxidized aromatic carbons at 136–153 ppm relative to the aliphatic region centered at 22 ppm than seen in stage 1. The overall ratio of carbonyl carbons (177 ppm) and aromatic carbons (130–153 ppm) to the aliphatic carbons centered at 22 ppm has changed in going from stage 1 to 3 from a value of 1.2–0.92, respectively. This change is primarily due to the production of oxidized aliphatic carbons seen in the 60–80 ppm range. Also, there is a diminution of the CH_3 resonances previously seen at 14 ppm in stage 1. These methyl groups are presumed to be converted to oxidized primary alcohols (~ 62 ppm). The spectrum of stage 5 is virtually identical with that of the selectively broadened ^{13}C spectrum of wood pulp (24). Nonprotonated resonances representing carbonyl, oxidized aromatic carbons, carbon-substituted aromatic carbons, methoxyl carbons (from lignin), and nonprotonated carbons are seen at 175, 153, 136, 57, and 20 ppm, respectively. After 3 months of composting and removal of residual wood chips, the spectrum of stage 7 in the dipolar-broadened form shows an increase in the ratio of aliphatic C–OH resonances to lignin-derived resonances as a consequence of the removal of excess wood chips and breakdown of residual carbohydrate (leaving the persistent lignin intact). All other relative areas have stayed approximately the same.

Fulvic and Humic Fractions. In order to evaluate the specificity of metal interactions in the sludge matrix, we examined the isolated humic and fulvic acid fractions derived from sludge stages 2 and 7. The iron content found in each of these fractions is given in Table VII. In each of the stages, as previously observed in the fractionation of whole soils, the fulvic fraction appears to bind the major quantity of metal (7, 8). This binding capacity is attributed to its hydrophilic nature (high carbohydrate content) and polyelectrolyte behavior (8). Such fulvic fractions are important for determining the eventual geochemical mobility of metals from sludge after its application to the soil.

Figure 8 compares the distribution of components found in each fraction derived from stage 2. ^{13}C spectra and relaxation data for the corresponding fulvic fraction from stage 7 could not be obtained due to its high metal and low overall carbon content. As predicted, fulvic acid fraction 2 is high in carbohydrate as well as iron. In contrast, humic acid fraction 2 has only about 12% of the iron found in fulvic 2,

and the ^{13}C spectra show significant amounts of aromatic material as well as carbohydrate. The carbonyl region of each spectrum shows a strong resonance due to carboxyl groups (179 ppm). The humic acid spectra bear a close resemblance to those of aquatic humins (23). The presence of lignin-type material is indicated by the OCH_3 resonance at 55 ppm. Both humic fractions (2 and 7) contain a large amount of aliphatic type carbon seen at ~ 22 ppm. These aliphatic resonances which are assigned primarily to long methylene chains may be strongly associated with carbohydrate moieties in the humic materials. An indication of this point is given by the fact that the proton T_1 values for both components are the same within experimental error (Table VII). If these structural components (carbohydrate and aliphatic) are covalently bound within this matrix, rapid proton spin diffusion could be responsible for the identical spin-lattice relaxation behavior. However, like the model system examined earlier, the carbohydrate protons undergo relaxation at a significantly faster rate than the aliphatic protons, due to their more intimate contact with the paramagnetic centers. The relaxation values of the carbohydrate resonances in stages 2 and 7 of Table VII are much longer than those corresponding to their humic and fulvic fractions. These extracts generally constitute less than 5% of the total material found at stages 2 and 7. Furthermore, the organic carbon present in the humic and fulvic acid of stages 2 and 7 represents an even lower percentage of the total carbon in these stages resulting in an extremely high paramagnetic/carbon ratio for the extracts. The overall contribution of these constituents to the macroscopic relaxation times observed for stages 2 and 7 will be negligible due to their minimal presence in the samples. However, these fractions do appear to show a strong affinity for iron binding and should be considered as geopolymers where significant amounts of paramagnetic ions may be localized.

From the relaxation data, paramagnetic iron appears to be preferentially associated with the humic 7 fraction relative to humic 2. The significant shortening of both proton T_1 and $T_{1\rho}$ values in humic 7 (Table VII) suggests that reactive functional groups capable of binding nine times the amount of iron have been generated in the humification process. A change in the structure of the aliphatic components as well as a possible speciation of the iron associated with this fraction is also indicated by a severely shortened aliphatic proton $T_{1\rho}$,

Registry No. Ligin, 9005-53-2; cellulose, 9004-34-6.

LITERATURE CITED

- (1) Schaumberg, G. D.; Levesque-Madore, C. S.; Sposito, G.; Lund, L. J. *J. Environ. Qual.* **1980**, *9*, 297.
- (2) Chaney, Rufus L., private communication.
- (3) Hartenstein, R. *Science* **1981**, *212*, 743.
- (4) Sposito, G.; Schaumberg, G. D.; Perkins, T. G.; Holtzclaw, K. M. *Environ. Sci. Technol.* **1978**, *12*, 931.
- (5) Norvell, W. A. "Micronutrients in Agriculture"; Soil Science Society of America, Inc.: Madison, WI, 1972.
- (6) Rawls, Rebecca L. *Chem. Eng. News* **1982**, *38*.
- (7) Gamble, D. S.; Langford, C. H.; Tong, J. P. K. *Can. J. Chem.* **1976**, *54*, 1239.
- (8) Saar, R. A.; Weber, J. H. *Environ. Sci. Technol.* **1982**, *16*, 510A.
- (9) Schnitzer, M. Proceedings of the International Peat Symposium, Bemidji State University, Bemidji, MN, 1981.
- (10) Stuermer, D. H.; Payne, J. R. *Geochim. Cosmochim. Acta* **1976**, *40*, 1109.
- (11) Worobey, B. L.; Webster, G. R. B. *Nature (London)* **1981**, *292*, 527.
- (12) Mikita, M. A.; Steelink, C.; Wershaw, R. L. *Anal. Chem.* **1981**, *53*, 1715.
- (13) Wershaw, R. L.; Mikita, M. A.; Steelink, C. *Environ. Sci. Technol.* **1981**, *15*, 1461.
- (14) Pines, A.; Gibby, M. G.; Waugh, J. S. J. *J. Chem. Phys.* **1973**, *59*, 569.
- (15) Schaefer, J.; Stejskal, E. O. *J. Am. Chem. Soc.* **1976**, *98*, 1031.
- (16) Barron, P. F.; Wilson, M. A.; Stephens, J. F.; Cornell, B. A.; Tate, K. R. *Nature (London)* **1980**, *286*, 585.
- (17) Barron, P. F.; Wilson, M. A. *Nature (London)* **1981**, *289*, 275.
- (18) Wilson, M. A.; Pugmire, R. J.; Zilm, K. W.; Kuan, M. G.; Heng, S.; Grant, D. M. *Nature (London)* **1981**, *294*, 648.
- (19) Wilson, M. A.; Barron, P. F.; Goh, K. M. *Geoderma* **1981**, *26*, 323.
- (20) Hatcher, P. G.; Rowan, R.; Mattingly, M. A. *Org. Geochem.* **1980**, *2*, 77.
- (21) Hatcher, P. G.; Schnitzer, M.; Dennis, L. W.; Maciel, G. E. *Soil Sci. Soc. Am. J.* **1981**, *45*, 1089.
- (22) Hatcher, P. G.; Breger, I. A.; Mattingly, M. A. *Nature (London)* **1980**, *285*, 560.
- (23) Hatcher, P. G.; VanderHart, D. L.; Earl, W. L. *Org. Geochem.* **1980**, *2*, 87.
- (24) Piotrowski, E. G.; Valentine, K. M.; Pfeffer, P. E. *Soil Sci.*, in press.
- (25) Sullivan, M. J.; Maciel, G. E. *Anal. Chem.* **1982**, *54*, 1606.
- (26) Mehring, M. "High Resolution NMR Spectroscopy in Solids"; Springer-Verlag: Berlin, 1976; p 138.
- (27) Opella, S. J.; Frey, M. H. *J. Am. Chem. Soc.* **1979**, *101*, 5854.
- (28) Epstein, E.; Wilson, G. B.; Burge, W. D.; Mullen, D. C.; Emkiri, M. K. *J. Water Pollut. Control Fed.* **1976**, *48*, 688.
- (29) Schnitzer, M.; Skinner, S. I. M. *Soil Sci.* **1968**, *105*, 392.
- (30) Ganapathy, A. N.; McDowell, C. A. *J. Am. Chem. Soc.* **1981**, *103*, 6011.
- (31) Brown, C. E. *J. Am. Chem. Soc.* **1982**, *104*, 5608.
- (32) Earl, W. L.; VanderHart, D. L. *Macromolecules* **1979**, *12*, 762.
- (33) Yoshida, T.; MaeKawa, Y.; Fujita, T. *Anal. Chem.* **1983**, *55*, 388.
- (34) Gerstein, B. C.; Ryan, L. M.; Murphy, P. D. *Prepr. Pap.—Am. Chem. Soc., Div. Fuel Chem.* **1979**, *24*, 90.

RECEIVED for review May 23, 1983. Accepted December 21, 1983.